Biomedical Microdevices 2:4, 295–303, 2000

Microfabricated Polysilicon Microneedles for Minimally Invasive Biomedical Devices

Jeffrey D. Zahn,[1,2] Neil H. Talbot,[1,3] Dorian Liepmann,[1,2,3] and Albert P. Pisano[1,3]

[1]Berkeley Sensor and Actuator Center, [2]Department of Bioengineering, [3]Department of Mechanical Engineering University of California at Berkeley, Berkeley, CA 94720

Abstract. **A two-wafer polysilicon micromolding process has been developed for the fabrication of hollow tubes useful for microfluidic applications. These small tubes can be fabricated with a pointed end, resulting in a micro hypodermic injection needle. Microneedles are desired because they reduce both insertion pain and tissue damage in the patient. Such microneedles may be used for low flow rate, continuous drug delivery, such as the continuous delivery of insulin to a diabetic patient. The needles would be integrated into a short term drug delivery device capable of delivering therapeutics intradermally for about 24 hours. In addition, microneedles can be used for sample collection for biological analysis, delivery of cell or cellular extract based vaccines, and sample handling providing interconnection between the microscopic and macroscopic world.**

The strength of microneedles was examined analytically, experimentally and by finite element analysis. Metal coatings provide significant increases in the achievable bending moments before failure in the needles. For example, a 10 µm platinum coating increased the median bending moment of a 160 µm wide, 110 µm high microneedle with a 20 µm wall from 0.25 to 0.43 mNm. In addition, fluid flow in microneedles was studied experimentally. Microneedles 192 µm wide, 110 µm high and 7 mm long have flow rates of 0.7 ml/sec under a 138 kPa inlet pressure. This flow capacity exceeds previous microneedle capacities by an order of magnitude.

Key Words. **microneedle, microfluidie, polysilicon, cromolding, drug delivery**

Introduction

In modern medical applications, there is a need for very small hypodermic needles that are economical to fabricate. Currently the smallest needles available, 30 gauge needles, have a 305 µm outer diameter with a wall thickness of 76 µm. Traditional machining methods make it unfeasible to create needles with a diameter less than 300 µm. Microneedles on the other hand can be any size and geometry since they are defined lithographically.

This new research builds upon the experience gained in previous research [1] and in this paper a new fabrication process is introduced which uses backside alignment to pattern one wafer on both sides. This eliminates a tedious wafer-to-wafer alignment step, and only a bare silicon wafer with a release layer needs to be bonded to the patterned wafer to create the closed passages. In addition, arrays of microneedles with multiple outlet ports have been fabricated using this process to allow the injection of different fluids from the same device, or the parallel extraction of fluid from many different sites (Figure 1).

Microneedles are also extremely sharp with sub-micron tip radii, whereas stainless steel needles can be comparably rough. This is because the fluid outlet is on the side of the needle rather than right at the tip like stainless steel needles.

In addition, it is impossible to create complex structures within a conventional needle. For example, a microfilter (Figure 2) cannot be placed inside of a traditional needle. Also, complex needle geometries such as 90° bends cannot be made with traditional machining since a metal needle will crimp when bent. Finally, highly parallel arrays of needles cannot be machined as a single part. However, since a the shape of a microneedle is defined lithographically all of these features can easily be incorporated into microneedle design.

Fluid flow rates is an import design criteria in order to meet dosage specifications of drugs A typical bolus injection for a diabetes patient is 0.3 ml. A patient can comfortably generate 138 kPa of pressure with a typical 0.5 cc disposable syringe. There are also many drugs which require only small doses. Analgesics such as Sufanta (Sufentanil Citrate), Sublimaze (Fentanyl Citrate), and Dilaudid (Hydromorphone) have doses of less than 3 µl per hour. Antibiotics such as Cefonicid, Ceftazidime, and Cefazolin Sodium are administered at a flow rate of ~ 0.16 ml per hour.

Early microneedles were made of single crystal silicon [2,3,4]. The device wafer was sacrificed or dissolved away in silicon etchant leaving the micro-needle behind. The fluid channels of these microneedles only occupy a small fraction of the interior volume of the needle resulting in a small fluid carrying capacity. These microneedles are useful for delivering fluid at low (< 0.1 µl/sec) flow rates but cannot deliver sufficient fluid for many therapeutic injections such as insulin.

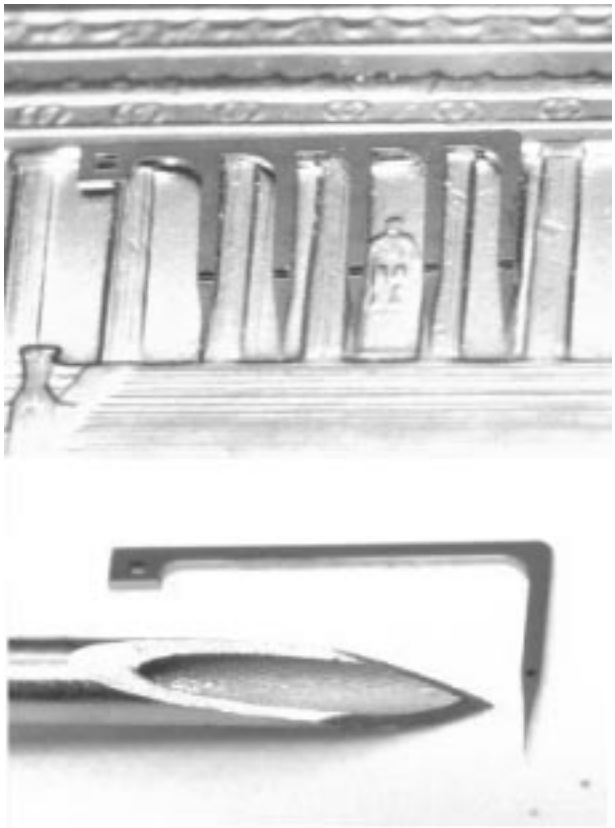

Fig. 1. (Top) Five barbed microneedle on the backside of a penny. (Bottom) ''Bent'' microneedle next to a 20 gauge stainless steel needle.

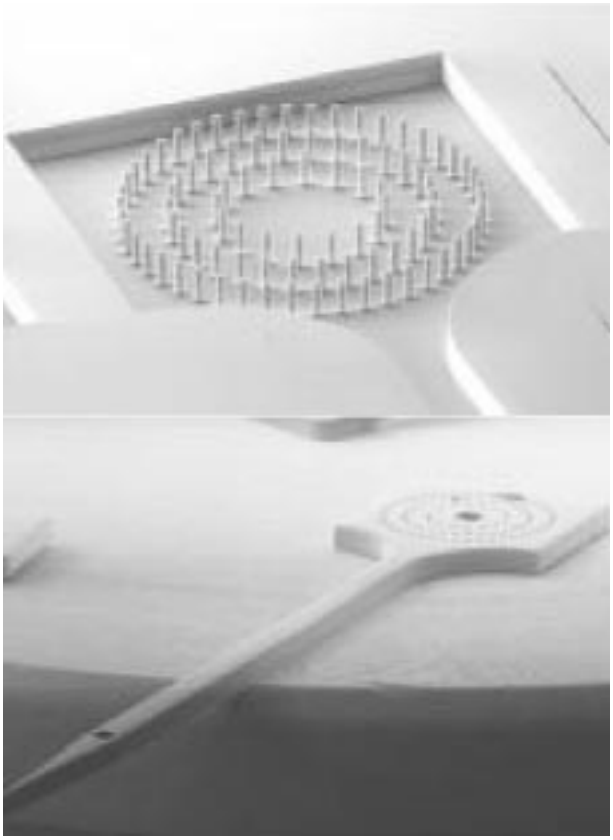

Fig. 2. (Top) SEM of a microneedle mold. (Bottom) SEM of a microneedle with a 6 mm shaft and a microfilter in its base.

Micromolded needles leave the majority of the interior volume free, and allow larger fluid flow rates for the same size needle outer diameter. Other approaches to microneedles have been investigated. One approach uses an SF_6/O_2 plasma to create high aspect ratio barbs for piercing the skin to allow therapeutics to diffuse across the skin [5–7]. However, these needles are not sufficient for injecting large amounts of fluids or clinically relevant dosages of many therapeutics.

Another approach uses electroplated palladium as the needle structural material and thick photoresist to define the needle channel [8–10]. However, because these needles are electroplated, they have very blunt tips.

Future work needs to be preformed to determine the biological response to needles. The first response to tissue distress from needle insertion is an inflammatory response at the insertion site [11]. During this time there may be tissue edema, which may affect delivery from the needles, and the migration of leukocytes to the injury site. Protein adsorption to the surface of the silicon will promote adhesion of leukocytes to the needles. Surface modifications of silicon surfaces to reduce protein adsorption is an active area of research. Some surface modifiers include: silicon carbide [12], polyethylene glycol (PEG) [13], or plasma enhanced chemical vapor deposition (PECVD) of a teflon-like fluropolymer. Any of these coatings could be incorporated into needle fabrication to improve biocompatability.

Since microneedles are designed for short term intradermal drug delivery, fibrous encapsulation is not expected because the needle is not inserted long enough for encapsulation to occur. Thrombosis is also not expected since the needle will not be in contact with the blood stream.

Due to the small size of microneedles, strength and robustness are the major factors in determining the range of their applications. Needles must be able to tolerate forces associated with insertion, intact removal and normal human movements if they are to be integrated into portable biomedical devices.

Fabrication

Molded microneedles use patterned mold wafers, similar in concept to Keller and Howe [14], that are not

sacrificed during the fabrication process. Therefore, many different designs of needles may be made, and the mold may be reused numerous times at a cost saving compared to sacrificial processing techniques.

Microneedles have been fabricated as previously reported [1]. The fabrication scheme has been modified so that instead of patterning two wafers separately, a single wafer is patterned on both sides (Figure 3). This eliminates the tedious step of wafer-to-wafer alignment. In addition, the microneedle design has been expanded to create arrays of parallel needles.

A double polished silicon wafer (*p*-type ⟨100⟩ single crystal) is used as a starting material as shown in Figure 3. The wafer is wet oxidized at 1,000°C to grow 1 μm of thermal oxide. The needle shapes are patterned using standard lithographic techniques and the patterned oxide is etched with reactive ion etching (RIE). The wafer is then coated with 0.3 μm of low pressure chemical vapor deposition (LPCVD) low stress silicon nitride. The backside of the wafer is aligned and patterned to the needle design using a Karl Suss contact mask aligner with backside alignment capabilities. The silicon nitride and oxide films are then etched away using RIE leaving a through hole mask. Afterwards the through holes are etched with potassium hydroxide (KOH). The nitride is then removed in phosphoric acid at 175°C. The needle mold is then etched using deep reactive ion etching (DRIE) in a surface technology systems (STS) etcher. The resulting trench is typically between 100 and 125 μm deep. The wafer is then wet oxidized at 1,000°C to decrease surface roughness. Afterwards 2 μm of phosphosilicate glass (PSG) is deposited onto the mold wafer. A second bare silicon wafer is coated with 2 μm of PSG. These two wafers are pressure bonded at 1,000°C in a nitrogen atmosphere. By patterning one wafer on both sides we no longer need to align wafers. After bonding,

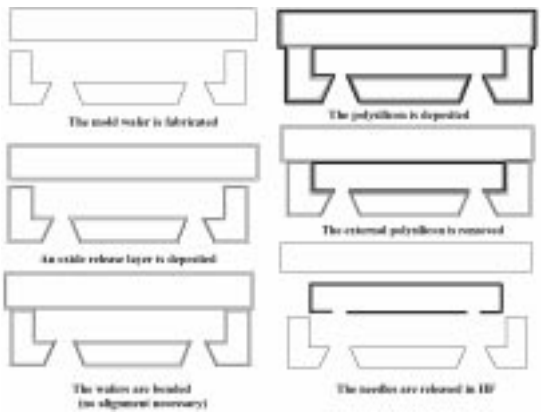

Fig. 3. *Improved fabrication scheme for making microneedles using a single wafer patterned on both sides.*

4 μm of polysilicon is deposited onto the mold wafers at, 580°C. The molds are then annealed at 1,000°C in a N_2 atmosphere. The polysilicon is annealed between depositions to alleviate film stress. The deposition and annealing is repeated until the desired thickness is reached, typically 15–20 μm. The polysilicon deposits conformally onto the outside of the wafer and inside the mold through the KOH etched through holes. After deposition, the external polysilicon is removed by RIE. The needles are then released in concentrated HF overnight.

Some needles were coated with metals to improve their strength. Three metals were chosen to compare how they affect needle strength. Titanium and platinum were sputtered onto microneedles in a Randex RF sputterer. The titanium film was deposited at 15 mTorr chamber pressure, 225 W forward power and 250 sccm argon. Platinum was deposited at 15 mTorr chamber pressure, 200 W forward power and 200 sccm argon. The needle metallization was either 10 μm of platinum or and 5 μm titanium. The needles were sputtered on one side, then turned over and sputtered on the other side. The deposition rate on the side walls was approximately half of the deposition rate on the horizontal surface. The film thickness was uniform on all surfaces because the side walls were exposed for twice as long as the top and bottom of the needles. The film thickness uniformity was verified by direct observation.

Some needles were also coated with electroplated nickel. An adhesion layer of chromium and gold was deposited by evaporation. First, 5 nm of chromium was deposited using a Veeco 401 resistance heated evaporator. Then without breaking vacuum 100 nm of gold was then deposited. The needles were then flipped over and coated on the other side. The needles were electroplated in a nickel sulfate solution composed of 200 g/L nickel sulfate, 5 g/L nickel chloride and 25 g/L boric acid. A DC current of 25 mA was applied for 30 minutes at 23°C for up to 30 minutes. The cathode current density was 30 mA/cm^2. This resulted in a 20 μm thick coating on the needles.

Finally, some needles were oxidized to inhibit crack initiation. Released microneedles were placed in an oxidation furnace and wet oxidized at 1,100°C for two hours resulting in about 1 μm of silicon dioxide on the exposed surfaces of the microneedles.

Theory

Microneedle strength

Since polysilicon is a ceramic material, the cause of needle fracture is crack initiation and propagation. Crack initiation can occur at any defect in the microneedle.

Since crack propagation is difficult to stop, the best approach is to inhibit crack initiation.

The first step is to try to make the surface of the microneedle as smooth as possible to avoid surface flaws. The PSG release layer determines the surface smoothness of the microneedle. When heated to 1,000°C PSG reflows and becomes very smooth. During the annealing process, phosphorus from the PSG diffuses into the polysilicon needle wall. It has been well documented that annealing of polysilicon films lowers residual stress, while phosphorus doping from PSG layers during the annealing process put a polysilicon film in compression [15]. Therefore, there should be a residual compressive stress on the surface of the needle. Compressive stress helps stop crack propagation by working against tensile stresses imposed on the surface of the needle by external loads during needle insertion into tissue.

Several possible failure modes of microneedles (buckling, shear, and bending) were modeled. Based upon these calculations, the major mode of failure for polysilicon microneedles is thought to be bending induced fracture.

The first possible failure mode considered was buckling. When a microneedle penetrates a tough membrane there is a short period of time when the microneedle is under compressive stress. During this time, if the second moment of area of the microneedle is not high enough relative to its length, the microneedle will buckle and break.

In order to address the issue of buckling in microneedles it is necessary to determine whether the buckling will be short-column or long-column buckling. For the Euler equation for long elastic columns of length L to be applicable the slenderness ratio L/k as defined below must be greater than the critical slenderness ratio

$$\left(\frac{L}{k}\right) = \sqrt{\frac{\pi^2 EA}{4F_{cr}}} \tag{1}$$

where E is the Young's modulus, A is the area and F_{cr} is the critical force that will cause short-column buckling. The radius of gyration k is defined as

$$k = \sqrt{\frac{I}{A}} \tag{2}$$

where I is the second moment of area. The critical slenderness ratio is defined as

$$\left(\frac{L}{k}\right)_{cr} = \sqrt{\frac{\pi^2 E}{2\sigma_y}}. \tag{3}$$

Using a Young's modulus of 169 GPa and a yield strength, σ_y, of 1.2 GPa for polysilicon, the critical slenderness ratio is 26. The slenderness ratio for a typical microneedle is 114. This result makes it clear that microneedles can be modeled as long columns and the Euler equation for elastic buckling can be applied

$$F = \frac{C\pi^2 EI}{L^2}. \tag{4}$$

Where F is the force and C is the end condition. In the computations, the base of the microneedle is modeled as a fixed joint while its tip is modeled as a pivoted slider which results in an end condition constant C of 0.25. Note that the fracture strength of polysilicon is not in the above equation; the critical variable is actually the second moment of area

$$I = \frac{BH^3 - bh^3}{12} \tag{5}$$

where B is the outer width of the microneedle and H is the outer height; b and h are the internal width and height of the fluid channel inside the microneedle.

Since the height H and h are raised to the third power in the second moment of area equation, they have the dominant effect. The typical height (H) was 110 μm making these microneedles very stiff compared to microneedles made by other microfabrication techniques. The width of the microneedle was 160 μm, while the wall thickness was 20 μm. The resulting critical buckling load for a 4.5 mm long microneedle is 0.30 N.

Shear is another possible failure mode that was considered for microneedles. In this analysis the maximum shear force V is approximated as half the yield strength σ_y multiplied by the material area A

$$V = \frac{\sigma_y A}{2}. \tag{6}$$

Stress concentration factors are not considered, so the results here are interpreted with caution. The calculated maximum shear load is 2.3 N. Except for combined loading situations as discussed later, this result indicates that other failure modes such as buckling or bending are more likely to occur.

In an ideal situation a microneedle would be inserted with a completely axial force with negligible bending moment. However, in real applications there is a large chance that the needle would experience a bending moment generated by a transverse tip force, itself due to misalignment as the needle is inserted. The needle was modeled as a cantilevered beam to approximate the transverse force and bending moment a needle could support. The maximum bending stress is therefore

$$\sigma = \frac{Mc}{I} \tag{7}$$

where c is the distance from the neutral axis to the outermost edge of the microneedle and M is the bending moment; I is the second moment of area as defined earlier. By replacing the bending moment with the tip force F multiplied by the needle length, L, we can solve for the maximum transverse tip force the needle can support

$$F = \frac{\sigma_y I}{cL} \tag{8}$$

where σ_y is the yield strength of polysilicon.

We assume that the strain distributions are linear and that Hooke's Law is valid. A 160 μm wide, 110 μm high microneedle with a 20 μm wall thickness and a 4.5 mm shank was analyzed. The maximum transverse tip force for this microneedle was computed to be 0.069 N which is equivalent to a bending moment of 0.31 mNm for this microneedle. These computations compare favorably with the experimental results. Since, for a given yield strength, the maximum supportable tip load due to the transverse tip force is less force than the maximum load generated by either shear or buckling, we conclude that bending is the critical mode of failure.

For microneedles which were coated with nickel, platinum and titanium to improve their strength the composite beam bending equation determines the critical load.

$$F = \frac{\sigma_y (E_{Si} I_{Si} + E_{Mt} I_{Mt})}{L c_{Si} E_{Si}} \tag{9}$$

where σ_y is still the yield strength of polysilicon, E refers to Young's modulus, and the subscripted *Si* or *Mt* refer to silicon or metal respectively.

Flow characteristics

It is important to model fluid flow characteristics in microneedles. The transition between laminar and turbulent flow is typically considered to occur at a Reynolds number $Re = UD_h/\upsilon = 2,300$, where U is the mean flow velocity through the needle, D_h is the hydraulic diameter (4 A_{cs}/Perimeter) and u is the kinematic viscosity. The experimental Reynolds number is well below the transition Re.

The pressure losses due to flow down a microneedle can be split into three categories: entrance losses, pressure decrease due to the drag that fully developed flow exerts on the duct walls, and losses due to specific microneedle geometry (expansions, bends, etc.).

For fully developed flow in the laminar regime the x-directed velocity profile in a rectangular duct with y and z cross section is given by

$$Vx(y,z) = \frac{16a^2}{\mu\pi^3}\left(-\frac{dP}{dx}\right)\sum_{i=1,3,5\ldots}^{\infty}(-1)^{(i-1)/2}\left[1-\frac{\cosh(i\pi z/2a)}{\cosh(i\pi b/2a)}\right]\frac{\cos(i\pi y/2a)}{i^3}$$
$$-a \le y \le a$$
$$-b \le z \le b \tag{10}$$

where $2a$ is the length of one of the walls, and $2b$ is the length of the other wall. Integrating this profile across y and z gives the average flow rate, Q as

$$Q = \frac{4ba^3}{3\mu}\left(-\frac{dP}{dx}\right)\left[1-\frac{192a}{\pi^5 b}\sum_{i=1,3,5\ldots}^{\infty}\frac{\tanh(i\pi b/2a)}{i^5}\right]. \tag{11}$$

The average velocity, U, is $Q/(4ab)$.

The pressure drop in the entrance region is estimated using the Blasius boundary layer solution over a flat plate

$$\tau_s = \frac{0.332\mu U}{x}\sqrt{Re_x} \tag{12}$$

where x is the distance along the plate and Re_x is the Reynolds number based on this distance. If it is assumed that a rectangular duct behaves as a collection of four plates then the pressure gradient can be estimated as

$$\frac{dP}{dx} = -\frac{4\tau_s}{D_h} \tag{13}$$

and the entrance pressure drop is found by integrating

$$\Delta P_{ent} = \int_0^l \frac{4}{D_h}\tau_s dx = \frac{4 * 0.332}{D_h}\sqrt{\rho\mu U^3}\int_0^l x^{-\frac{1}{2}}dx$$
$$= \frac{8 * 0.332}{D_h}\sqrt{\rho\mu U^3 l} \tag{14}$$

where l is the entrance length or the needle length, whichever is shorter.

The entrance length is defined as the point where the pressure gradient was matched to that of the fully developed flow

$$\frac{dP}{dx} = -\frac{4\tau_s}{D_h} = \frac{-Q}{\frac{4ba^3}{3\mu}\left[1-\frac{192a}{\pi^5 b}\sum_{i=1,3,5\ldots}^{\infty}\frac{\tanh(i\pi b/2a)}{i^5}\right]}. \tag{15}$$

It should be noted that this entrance length estimate is about 20% of the standard macroscopic entrance length estimate of

$$\frac{l}{D_h} = 0.59 + 0.055\ Re. \tag{16}$$

Next the losses due to viscous drag on the walls of the needle and geometric effects are modeled by applying

the Modified Bernoulli equation. The pressure drop across the needle is

$$\Delta P = \Delta P_{ent} + \frac{1}{2}\rho\left(U_2^2 - U_1^2\right) + f\frac{L}{D_h}\frac{1}{2}\rho U^2 + K_{geom}\frac{1}{2}\rho U^2 \quad (17)$$

where L is the needle length minus the entrance length. The fraction factor, f, is

$$f = \frac{4|\Delta P_{dev}|}{\rho U^2}\frac{D_h}{L} \quad (18)$$

where ΔP_{dev} indicates the fully developed pressure drop. K_{geom} is the geometric loss factors, which for a bent needle is

$$K_{geom} = 1.3 \quad (19)$$

while for a sudden contraction

$$K_{geom} = \left(\frac{2}{m} - \frac{A_2}{A_1} - 1\right)$$

where m is the root of the quadratic

$$\frac{1 - m(A_2/A_1)}{1 - (A_2/A_1)^2} = \left(\frac{m}{1.2}\right)^2 \quad (20)$$

and where A_1 and A_2 are the cross sectional areas before and after the contraction respectively.

Experimental Apparatus

Microneedles were tested and the maximum bending moment was determined for each microneedle. The breaking strength of each microneedle was tested with a mechanical force gauge. The force gauge had a range of 0–20 g and an accuracy of 0.1 g. Microneedles were mounted on a glass slide using a cyanoacrylate ester adhesive. The base was attached to the slide with the tip and shank cantilevered off the edge of the slide (Figure 4). The microneedles were tested for bending in the vertical direction since this is the predicted failure mode. After mounting, the glass slide was clamped and the force was incrementally increased on the tip of the needle until it fractured. For constancy of results all needles tested were from a single fabrication batch.

The fluid flow characteristics of the microneedles were also studied. The experimental setup comprised a pressurized air source, pressure regulator, pressure gauge, and a 20 ml graduated pressure vessel. Air source was supplied at 300 kPa, and the regulator was used to supply a constant pressure of 138 kPa which is a representative pressure a patient can generate in a 0.5 ml syringe. The graduated pressure vessel was filled with water and attached to the pressure source with tygon tubing and an intervening valve. Flow rate was determined by timing the water level change in the graduated pressure vessel.

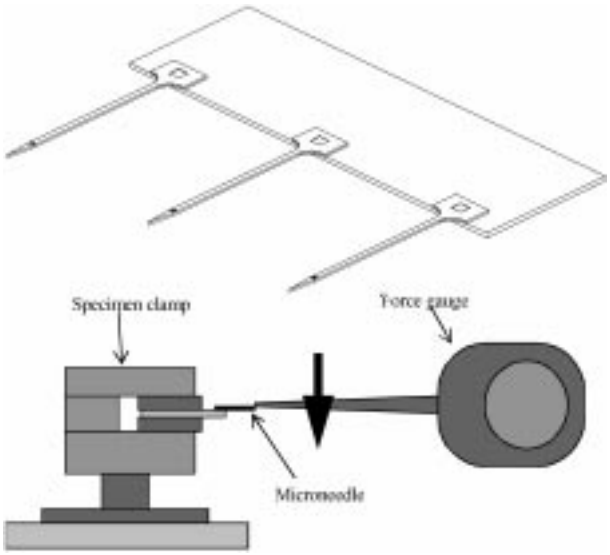

Fig. 4. *(Top) Microneedles mounted on a microscope slide for strength testing. (Bottom) Experimental setup for strength tests.*

Results and Discussion

Experimental strength tests indicate that metal coatings raise the median maximum bending moment a needle can support (Figure 5). In addition, metal coatings are desired because they can deform plastically rather than fracturing. Thus the metal coating may hold a needle together for extraction even after the needle breaks (Figure 6). Sputtered films are preferred over electroplating, since electroplating blunts the tips of the needles. Different metals were chosen to study their strength improvement. However, titanium is the most logical coating choice since it is the most biocompatible. No strength improvement was seen from oxidizing microneedles. This may be because the surface of the microneedle was already under compressive stress due to phosphorous doping. It should be noted that the actual strength of needles is lower than the theoretical values. This is because theory assumes a continuous material with no defect or inclusions which act as crack propagation sites. In reality, polysilicon has defects so the experimental strength is lower than the theoretical. Defects also account for the distribution in the experimental data Table 1.

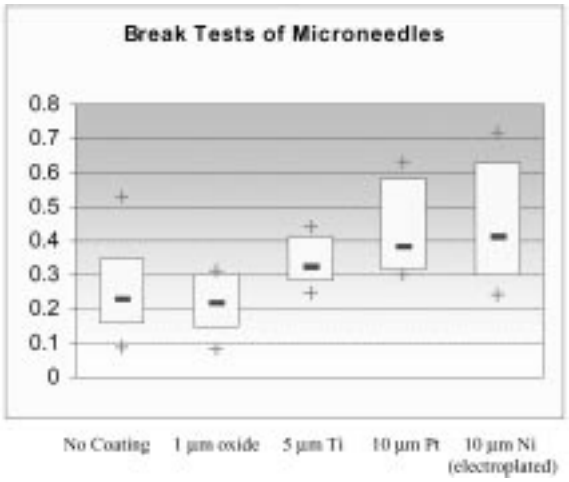

Fig. 5. *Break tests of sets of microneedles for various metal coatings. The dash (–) represents data median. The box represents the 25 and 75% confidence limits, and the cross (+) shows the 5 and 95% confidence limits.*

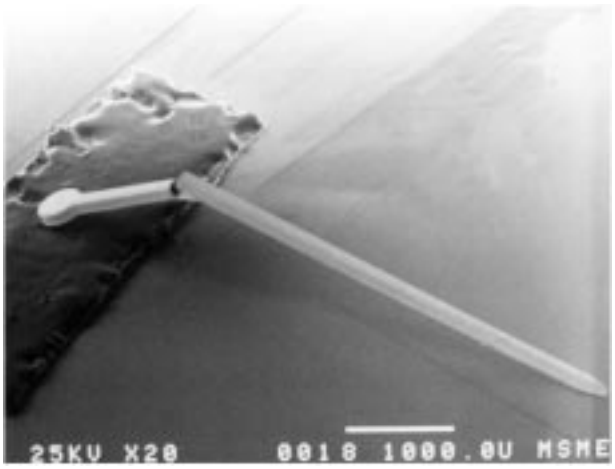

Fig. 6. *Fractured microneedle being held together by its platinum coating.*

Cross batch variations in mechanical properties are also expected. depending upon deposition variables. Polysilicon mechanical properties are a strong function of deposition variables (temperature, pressure, silane flow rates, etc.). Therefore, consistency in variables during deposition is necessary to yield consistent material properties. A commercial process which has more consistent depositions should have less spread within the data. There should be less defects in the polysilicon, and the density of defects should be more consistent from needle-to-needle, and batch-to-batch.

Needle strength was also analyzed using a finite element model (ANSYS) of a needle. A representative simulation is shown in Figure 7. Both in-plane and out of plane tip loads were simulated and the Von Mises stresses were calculated. Von Mises stresses are a measure of total strain energy at any given point and takes into account all types of simultaneous loading. In the case of a cantilevered microneedle, the stresses due to bending and shear both contribute to the stress state at any given part of the needle. The analysis was done with out of plane tip loads of 10 g which results in a maximum stress of 1,878 MPa. By comparison, the bending stress for the same geometry was computed analytically at 1,778 MPa. The maximum stress is at a maximum near the fillet because the bending moment increases linearly from the tip of the needle to the base. The stress decreases in the fillet as the load is being progressively spread over a wider cross section. As expected the stress generated by (in plane) side loads were less than the out of plane load. The maximum Von Mises stress was 1,322 MPa. The reason for the lower stress is the needles are twice as wide (in plane) as they are high (out of plane).

In addition, the fluid carrying capacity of needles was examined. The bent microneedle was found to have the highest fluid carrying capacity of 0.082 ml/sec at 138 kPa with a Reynolds number of 708. A microneedle with a built in microfilter also had flow rates of 0.07 ml/sec. These needles could be used for bolus insulin injections. Other needles were found to have lower fluid carrying capacity which make them inadequate for bolus injections, but may be useful for long term ''IV drip style'' drug delivery systems. Although the throughput of these microneedles are low they still compare favorably with other microneedle designs. For example, the Lebouitz microneedle can only deliver 35 nl/sec. at 300 kPa [4]. Laminar flow models accurately predict the

Table 1. *Summary of microneedle strength computations and experimental results. The computed maximums are determined using equations (8) and (9)*

Microneedle coating type	Coating thickness (micrometers)	Sample size	Computed maximum moment (mNm)	Avg. measured maximum moment (mNm)	Standard deviation (mNm)
None	0	10	0.31	0.25	0.05
Oxide	1	4	0.31	0.22	0.06
Titanium	5	7	0.49	0.34	0.04
Platinum	10	7	0.59	0.43	0.08
Nickel	10	8	0.73	0.45	0.07

Table 2. *Experimental vs. predicted flow behavior. The predicted flow rate is determined by estimating the entrance length using equation (15), and then applying equation (17) to correlate pressure loss with flow rate*

Needle style	Number of tests	Avg. measured flow rate (cc/sec)	Computed flow rate (cc/sec)	Error (%)	Reynolds number
Bent, 90°	4	0.082 ± 0.004	0.088	7.3	738
Reinforced	9	0.040 ± 0.004	0.040	0.0	503
Filter	2	0.070 ± 0.01	0.083	17.9	688
Double channel	1	0.032	0.034	6.2	260

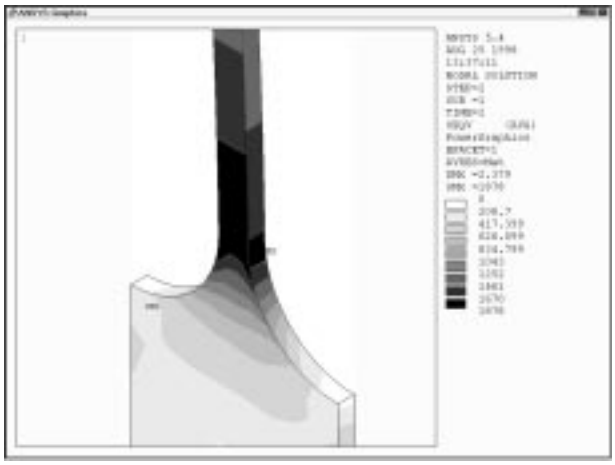

Fig. 7. *Finite Element Analysis of a cantilevered microneedle with a 10 g out-of-plane tip load.*

flow behavior through microneedles. The largest error occurred in the filter needles. This is because of the small gap spacing between the filter rungs (see Figure 2). This geometry is difficult to model and was simply assumed to be many short thin channels in a parallel arrangement. However, the model does show the significance of entrance and geometry losses as each was about 10% of the pressure loss through the needle. Therefore more effort should be placed on minimizing these effects in order to increase needle flow efficiencies. The results of the flow model are summarized in Table 2.

Conclusion

Polysilicon micromolding allows the fabrication of microneedles which are smaller, smoother, and sharper with more complicated geometries than needles made using traditional machining methods. In addition, these needles have features which would be difficult if not impossible to implement using other fabrication methods. Features such as three stage microfilters, barbs, bends, and multiple outlet ports have been implemented while maintaining good structural integrity and fluid flow characteristics. In addition, these needles could easily be housed in a casing similar to traditional injection needles, or integrated in an IV drip style microfabricated drug delivery system. Polysilicon microneedles make a model system for studying fluid dynamics on the microscale, biocompatability issues with microfabricated biomedical devices, and feasibility of microneedles for biomedical systems. Future directions of research include strengthening needles either by surface treatments or by fabricating needles out of alternative materials, biomedical device integration, and biomedical injection studies.

Acknowledgments

This work was funded by Becton Dickinson Technologies. The authors would like to extend a special thank you to Burton Sage. His inspired vision contributed to making this work possible. The authors would like to thank Chris Keller for his help in technology development. We would also like to acknowledge George Dougherty for his help with ANSYS computer simulations. Finally, we would like to thanks all members of the Liepmann/Pisano labs for helpful discussions. All devices were fabricated at the University of California, Berkeley microfabrication facilities.

References

1. N. Talbot and A.P. Pisano, Proceedings 1998 Solid State Sensor and Actuator Workshop Hilton Head, S.C., 25–268, (1998).
2. L. Lin, A.P. Pisano, and R.S. Muller, Solid State Sensors and Actuator Conference, Transducers '93, Japan, 237–240 (1993).
3. J. Chen and K.D. Wise, Solid State Sensor and Actuator Workshop, Hilton Head, S.C., 256–259 (1994).
4. K.S. Lebouitz and A.P. Pisano, Proceedings Microstructures and Microfabrication Systems IV, 194th meeting of the Electrochemical Society, Boston, MA, 1–6 (1998).
5. S. Henry, D.V. McAllister, M. Allen, and M. Prausnit, Proceedings of the IEEE Eleventh Annual International Workshop on MEMS, Heidelberg, Germany, 494–498 (1998).
6. D.V. McAllister, F. Cros, S.P. Davis, L.M. Matta, M.R. Prausnitz, and M.G. Allen, Transducers '99, 1098–1101 (1999).
7. D.V. McAllister, S. Kaushik, P.N. Patel, J.L. Mayberry, M.G. Allen, and M.R. Prausnitz, Proceedings of the First Joint BMES/EMBS Conference, Atlanta, GA, USA, 13–16 Oct. 1999; Piscataway, NJ, USA, IEEE, 1999 **2,** 836.

8. I.E. Papautsky, J.D. Brazzle, H. Swerdlow, and A.B. Frazier, IEEE International Conference on Engineering in Medicine and Biology Conference, (Chicago, IL, 1997).
9. J. Brazzle, I. Papautsky, and A.B. Frazier, IEEE Engineering in Medicine and Biology Magazine, **18**(6), 53–58 (IEEE, 1999).
10. J. Brazzle, D. Bartholomeusz, R. Davies, J. Andrade, R.A. Van Wageman, and A.B. Frazier, Proceedings 2000 Solid State Sensor and Actuator Workshop Hilton Head, S.C., 199–202 (2000).
11. J.E. Lemons, F.J. Schoen, A.S. Hoffmann, and B.D. Rater (eds), *Biomaterials Science: An Introduction to Materials in Medicine*, (Academic Press, San Diego, CA., 1996), 165–173.
12. A. Bolz and M. Schaldach, Medical and Biological Engineering and Computing **31**, Suppl:S123–S130 (1993).
13. M.Q. Zhang, T. Desai, and M. Ferrari, Biomaterials **19**(10), 953–960 (1998).
14. C.G. Keller and R.T. Howe, International Solid State Sensors and Actuator Conference. Transducers '95, Stockholm, Sweden, 376–379 (1995).
15. P. Krulevitch, G.C. Johnson, and R.T. Howe, Mat. Res. Soc. Symp. Proc. **276**, 79–84 (1992).